

Phase separation frustrated by the long range Coulomb interaction I: Theory

J. Lorenzana,^{1,2} C. Castellani,¹ and C. Di Castro¹

¹ *Dipartimento di Fisica, Università di Roma "La Sapienza" and Istituto Nazionale di Fisica della Materia, Unità di Roma I, Piazzale A. Moro 2, I-00185 Roma, Italy.*

² *Consejo Nacional de Investigaciones Científicas y Técnicas, Centro Atómico Bariloche, 8400 S. C. de Bariloche, Argentina (October 28, 2018)*

We analyze the combined effect of the long range Coulomb (LRC) interaction and of surface energy on first order density-driven phase transitions between two phases in the presence of a compensating rigid background. In the coexistence region we study mixed states formed by regions of one phase surrounded by the other in the case in which the scale of the inhomogeneities is much larger than the interparticle distance. Two geometries are studied in detail: spherical drops of one phase into the other and a layered structure of one phase alternating with the other. In the latter case we find the optimum density profile in an approximation in which the free energy is a functional of the local density (LDA). It is shown that an approximation in which the density is assumed to be uniform (UDA) within each phase region gives results very similar to those of the more involved LDA approach. Within the UDA we derive the general equations for the chemical potential and the pressures of each phase which generalize the Maxwell construction to this situation. The equations are valid for a rather arbitrary geometry. We find that the transition to the mixed state is quite abrupt i.e. inhomogeneities of the first phase appear with a finite value of the radius and of the phase volume fraction. The maximum size of the inhomogeneities is found to be on the scale of a few electric field screening lengths. Contrary to the ordinary Maxwell construction, the inverse specific volume of each phase depends here on the global density in the coexistence region and can decrease as the global density increases. The range of densities in which coexistence is observed shrinks as the LRC interaction increases until it reduces to a singular point. We argue that close to this singular point the system undergoes a lattice instability as long as the inverse lattice compressibility is finite.

Pacs Numbers: 64.75.1g 71.10.Hf 71.10.Ca

I. INTRODUCTION

The complex phase-diagrams of hole doped cuprates and manganites have rekindled the study of mixed states in modeling these systems.¹⁻³ Indeed strongly correlated systems with narrow bandwidth and short range interactions show a generic tendency to phase separate into hole-rich and hole-poor regions. When long range Coulomb (LRC) forces are taken into account this instability with macroscopic separation is frustrated due to the electrostatic energy cost and this can lead to charge inhomogeneous states of various nature,⁵⁻⁸ where domains of various forms of one phase (B) are embedded in the other phase (A).

In the inhomogeneous state the charge is segregated locally over some characteristic distance but the overall density (averaged over much larger distances) is a fixed constant in order to guarantee large scale neutrality and avoid the large Coulomb cost. Such a segregation has been considered at a scale comparable to the interparticle distance to explain the origin of striped states in cuprates.^{7,8}

In this work we will consider the opposite case in which the scale of the inhomogeneities is much larger than the interparticle distance. We consider in particular two different kinds of inhomogeneities: spherical drops of one phase into the other phase and alternating layers of each

phase. The first case has been pioneered by Nagaev and collaborators in the context of doped magnetic semiconductors in general and of manganites in particular.^{5,6} Related ideas have been recently presented in Refs. 3,9.

We believe that for the general understanding of the large scale inhomogeneous state the specific mechanism producing phase separation (PS) in the absence of LRC forces is rather unessential. Of course specific short range interactions in each physical system will lead to different A and B phases (which will also depend on the doping regions one considers) giving rise to different physical situations. However, in the same spirit of the Maxwell construction, one can perform a general analysis of the phenomena due to the tendency towards PS in the presence of Coulomb interaction irrespectively of the microscopic mechanisms of PS itself.

We consider two charged phases A and B with a compensating rigid background and we study the formation of inhomogeneous states in a density-driven first-order phase transition between A and B . By definition A and B have different densities; one of the phases is undercompensated and the other is overcompensated by the background. It follows that the inhomogeneities are charged and they repel each other. Since the inhomogeneities are formed by many particles, quantum effects are negligible and they crystallize.⁴ The drops arrange in a Wigner crystal whereas the layers form a periodic structure. We

restrict to three dimensional (3D) textures. A large number of small inhomogeneities minimize the Coulomb energy but they cost too much surface energy. The distance between the inhomogeneities and their size are found by minimizing a free energy which takes into account both these effects.^{5,6}

In ordinary PS the Maxwell construction (MC) is invoked to find the range of density $n_A^0 < n < n_B^0$ in which a system prepared with the overall density n separates in two regions with densities n_A^0 and n_B^0 respectively. We generalize here the MC and derive the equations that should be satisfied in the mesoscopically inhomogeneous coexistence region by the chemical potential and the pressure of each phase (Sec. II). To this end we use an approximation in which the density within each phase is assumed to be constant which we name uniform density approximation (UDA). We solve the equations for the drop geometry in the simple (but general enough case) in which the free energy of both the A and B phases can be approximated by a parabola (Sec. III).

We define a coupling constant λ given by the ratio between the energy cost due to surface energy plus the LRC interaction and the energy gain in MC PS. Only below a critical value λ_c PS is possible. Above λ_c the system is uniform A (B) phase below (above) a critical density with a lattice instability close to the critical density.

The characteristic size of the inhomogeneities is shown to be of order $\sqrt{\lambda}l_s$ with l_s an electric field screening length. Since λ is bounded by λ_c (of order 1) it follows that the inhomogeneities are of the order of or less than l_s .

For small volume fraction the drop geometry is more stable than the layers as expected from general surface energy arguments. On the other hand the layered geometry being simpler serves as a ground test for approximations. In order to validate the UDA we solve the layered geometry in the UDA and in the more general case in which the density profile can spatially vary within each phase. In this last case the density profile is allowed to adjust minimizing a free energy which is an approximate functional of the local density (LDA). Both the UDA and the LDA are shown to give very similar results for averaged quantities (Sec. IV A).

To illustrate the generality of these ideas we consider some applications in paper II of this series.

II. FREE ENERGY AND COEXISTENCE EQUATIONS: THE UNIFORM DENSITY APPROXIMATION

We consider a density-driven first order phase transition in the presence of the LRC interaction and surface energy. We look for the formation of a mixed state by increasing the density from the uniform A phase. We use two different geometries for the mixed state. i) The drop geometry consist of a Wigner crystal of drops of B phase

in the host phase A . ii) The layered geometry is made of a periodic array of alternating layers of A and B phases.

For both geometries the electronic density within each single phase region is taken as uniform (UDA) and in general it will result different from the compensating background density. This is of course an approximation since both densities will tend to adjust within each phase also to make the total electrochemical potential constant. The UDA will be relaxed in Sec. IV for the layered geometry by minimizing a free energy functional on a simple LDA. We anticipate here that both the UDA and the LDA give very similar results thus justifying our extensive use of the UDA here and in paper II.

We start by computing the total free energy. In the same spirit of the MC we assume that the free energies of hypothetically homogeneous bulk phases are known and given by F_A and F_B . We define the mixing energy E_m as the sum of the total surface energy and electrostatic energy (computed below). We work at a fixed total volume V and number of particles N . At a given temperature the total free energy is $F = F_B(V_B, N_B) + F_A(V_A, N_A) + E_m$. We have to minimize this respect to V_B and N_B subject to the conditions $V_B + V_A = V$, $N_B + N_A = N$. The volume fraction of B phase is $x \equiv V_B/V$. We can work with the free energies per unit volume $f \equiv F/V$, $e_m \equiv E_m/V$, $f_B \equiv F_B(V_B, N_B)/V_B$ and work with the densities $n_B \equiv N_B/V_B$ etc. so the function to minimize is:

$$f = (1-x)f_A(n_A) + xf_B(n_B) + e_m \quad (1)$$

The constraint in the number of particles is written as $n = xn_B + (1-x)n_A$ and the constraint in the volume is satisfied by putting $V_B/V = 1-x$. It is convenient to define $\delta \equiv n_B - n_A$ and to use the constraint in the number of particles to eliminate n_B and n_A in favor of n and δ .

In order to compute the mixing energy we first consider the drop geometry. We assume that the drops are spheres of radius R_d . This will be a good approximation as long as x is small and the crystal field is also approximately spherical. This is true for fcc, bcc and hcp lattices.^{10,11} To compute the electrostatic energy we use the Wigner-Seitz approximation.^{5,10,11} We divide the system in slightly overlapping spherical cells each one with the volume $4\pi R_c^3/3 = V/N_d$ where N_d is the number of drops and R_c is the radius of the cell. Fig. 1 shows a schematic view of the cell density profile.

Next we compute the electrostatic energy. The cells are globally neutral (by construction) and only the charge inside the cell contributes to the electric field in the cell.

The charge density of phase B is n_B (actually $-en_B$ but we drop the charge of the particles $-e$ for simplicity). The dashed background charge density in Fig. 1 ($-n_A$) compensates the A charge density n_A , and a slice of height n_A of the B charge density. For the purpose of computing the electrostatic energy these charge densities can be eliminated and one is left with the density

$n_B - n_A (= \delta)$ inside the drop and $-(n - n_A)$ for the background. We will call the former “drop contribution” and the latter the “background contribution”. There is no “host” contribution due to the above cancellation.

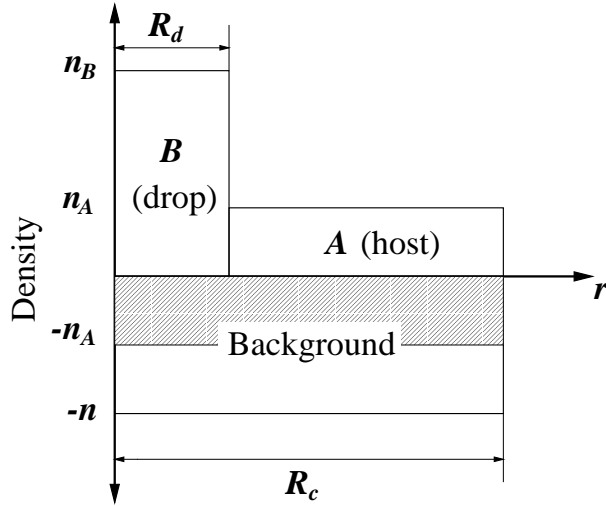


FIG. 1. Schematic view of a cell density profile in the UDA with a drop (layer) of B phase in the host A. The origin is at the center of the cell. The full cell diameter (width) is $2R_c$ for drops (layers). The dashed region of the background compensates the A density and part of the B density.

Another assumption is that the charge is spread uniformly and that microscopic discreteness effects can be neglected. One can see that corrections to the electrostatic energies due to discreteness are of order a^2/R_d^2 (Appendix. A) where a is the characteristic length of the microscopic structure (for example a lattice constant). Therefore they are negligible in our analysis which considers $R_d \gg a$.

With the above approximations the total electric field inside the cell is written as $\mathbf{E} = \mathbf{E}_b + \mathbf{E}_d$ where b (d) refers to the background (drop) contribution. Integrating the square of the electric field we obtain three contributions to the electrostatic energy: $\epsilon = \epsilon_d + \epsilon_b + \epsilon_{d-b}$ with

$$\epsilon_d = \frac{1}{8\pi\epsilon_0} \int d^3\mathbf{r} \mathbf{E}_d^2 \quad (2)$$

with ϵ_0 the static dielectric constant and a similar equation for the background. The interaction energy is

$$\epsilon_{d-b} = \frac{1}{4\pi\epsilon_0} \int d^3\mathbf{r} \mathbf{E}_b \cdot \mathbf{E}_d \quad (3)$$

The use of the static dielectric constant is well justified because we are assuming a static super structure which certainly will produce relaxation of the ions which in turn will screen the electric field. We are assuming by symmetry that the electric displacement is parallel to the electric field. The fields can be easily evaluated with Gauss theorem. One obtains

$$\epsilon_d = Q^2 \frac{3}{5\epsilon_0 R_d} \quad (4)$$

$$\epsilon_b = Q^2 \frac{3}{5\epsilon_0 R_c} \quad (5)$$

$$\epsilon_{d-b} = \frac{3Q^2}{\epsilon_0} \left(-\frac{1}{2R_c} + \frac{R_d^2}{10R_c^3} \right) \quad (6)$$

where $Q \equiv -e\delta v_d$ is the effective charge inside the drop. The volume of a drop is $v_d = 4\pi R_d^3/3$ and the number of drops is given by $N_d = V_B/v_d = xV/v_d$. We also have that $x = R_d^3/R_c^3$. Finally the total electrostatic energy per unit volume can be put as:

$$e_e = \frac{2\pi e^2 \delta^2}{5\epsilon_0} R_c^2 x^{5/3} (2 - 3x^{1/3} + x). \quad (7)$$

Setting one of the densities in δ to zero one recovers the expressions obtained by Nagaev and collaborators for the particular case of a mixed state composed of an antiferromagnetic insulating phase and a ferromagnetic metallic phase.^{5,6}

The surface energy is parametrized by a quantity σ with dimensions of energy per unit surface. In general σ will be a function of the densities n_A , n_B . The total surface energy per unit volume is:

$$e_\sigma = 4\pi\sigma R_d^2 \frac{N_d}{V} = \frac{3\sigma x^{2/3}}{R_c} \quad (8)$$

These two contributions add to the mixing energy per unit volume $e_m = e_e + e_\sigma$.

Due to the constrain we have three parameters to determine (δ , x , R_c). The mixing energy is the only contribution which depends explicitly on the geometry. We can therefore eliminate R_c in favor of δ and x by minimizing e_m respect to the cell radius to get:

$$R_c = \left(\frac{15\sigma\epsilon_0}{4\pi x(2 - 3x^{1/3} + x)e^2\delta^2} \right)^{1/3} \quad (9)$$

Now we consider the layered geometry. The cell consist of a layer of width $2R_c$. The center of the cell is occupied by a layer of width $2R_d$ of B phase and the rest is occupied by A phase. Fig. 1 serves as a schematic plot of the density profile also in this case. r is a coordinate perpendicular to the layers with the origin at the center of the B layer. The volume fraction now is given by $x = R_d/R_c$. By following analogous arguments as for the drops we obtain:

$$e_e = \frac{2\pi e^2}{3\epsilon_0} \delta^2 R_c^2 x^2 (1 - x)^2 \quad (10)$$

$$e_\sigma = \frac{\sigma}{R_c} \quad (11)$$

$$R_c = \left(\frac{3\sigma\epsilon_0}{4\pi x^2(1 - x)^2 e^2 \delta^2} \right)^{1/3} \quad (12)$$

Once R_c has been eliminated for both geometries the mixing energy can be put as:

$$e_m = \left[\frac{\sigma^2 e^2 \delta^2}{\epsilon_0} \right]^{1/3} u(x) \quad (13)$$

where all the geometric information is stored in $u(x)$:

$$u(x) = 3^{5/3} \left(\frac{\pi}{10} \right)^{1/3} x(2 - 3x^{1/3} + x)^{1/3} \quad (\text{drops}) \quad (14)$$

$$u(x) = \left(\frac{\pi}{2} \right)^{1/3} [3x(1-x)]^{2/3} \quad (\text{layers}) \quad (15)$$

In Fig. 2 we plot $u(x)$.

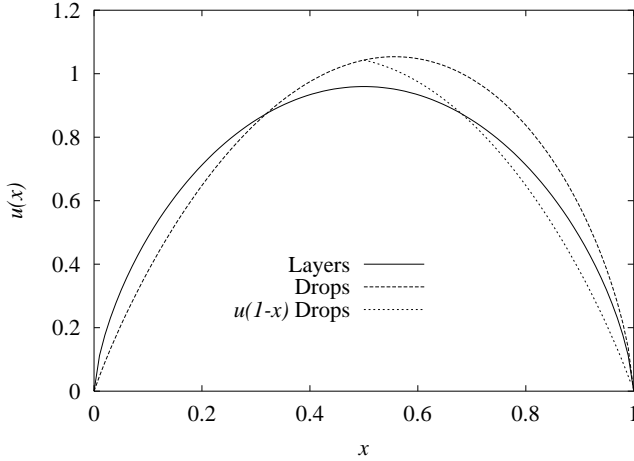


FIG. 2. The function $u(x)$ that parameterizes the mixing energy for the layer geometry and the drop geometry.

The free energy should remain invariant respect to an exchange of the kind $A \leftrightarrow B$ and $x \leftrightarrow 1 - x$. We will term this as “phase exchange symmetry”. Fig. 2 shows that this symmetry is only approximately realized by the $u(x)$ for drops. The deviation is due to the fact that the surface energy is minimized when the minority phase inhomogeneities are spherical. Our drop solution imposes this at small x but violates this in the opposite case of $x \rightarrow 1$ where the minority phase inhomogeneities have the complicated geometry between the spherical drops. In practice, however, our approximations can be meaningful even at intermediate and large x because the present $u(x)$ is approximately symmetric around $x = 1/2$. This is due to the fact that the electrostatic energy Eq. (7) correctly cancels in this limit driving the total mixing energy to zero.

A better treatment should allow at $x > 1/2$ for a switch from the unoptimized interstitial geometry to a spherical geometry with an energy gain given by the reflected $u(x)$ at small x in $u(1-x)$ as shown in Fig. 2. A comparison between the reflected curve and the original $u(x)$ shows that this geometry optimization compared with an apparently very bad geometry gives rise to a modest lowering of the energy. The same happens when we switch from the layer geometry to the spherical drop geometry

as shown in Fig. 2. We can conclude that the dependence on geometry is weak.

The spheric drop geometry has lower energy than the layered geometry as expected from general arguments on surface tension. The exception is close to $x = 1/2$ where our spherical drop solution is not adequate in any case. In fact in this region drops and the crystal potential will be far from spherical. The problem of establish the optimum geometry close to $x = 1/2$ is beyond the scope of this work however we expect minor corrections to thermodynamic quantities due to the small sensibility of $u(x)$ to dramatic changes in the geometry as illustrated above.

Although the layer solution has higher energy due to its simplicity it is an excellent test ground for checking the approximations. We take advantage of this fact to test the UDA approximation in Sec. IV A. In addition the layer geometry has the extra advantage that, by construction, respects the phase exchange symmetry.

Anyway since $u(x)$ depends weakly on geometry our results for macroscopic thermodynamic quantities will be largely independent of the geometry itself. When possible we present our results in a geometry independent way by leaving the function $u(x)$ unspecified in our expressions.

Minimizing the free energy respect to δ and x one obtains:

$$\mu_B - \mu_A = -\frac{2(e\sigma)^{2/3}u(x)}{3(\epsilon_0\delta)^{1/3}x(1-x)} + \frac{2(e\delta)^{2/3}u(x)}{3\epsilon_0^{1/3}\sigma} \left(\frac{1}{x} \frac{\partial\sigma}{\partial n_A} - \frac{1}{1-x} \frac{\partial\sigma}{\partial n_B} \right) \quad (16)$$

$$p_B - p_A = (\mu_B - \mu_A)[n + \delta(1-2x)] + \left(\frac{e^2\sigma^2\delta^2}{\epsilon_0} \right)^{1/3} u'(x) - \frac{2\delta^{5/3}e^{2/3}u(x)}{3(\epsilon_0\sigma)^{1/3}} \left(\frac{\partial\sigma}{\partial n_A} + \frac{\partial\sigma}{\partial n_B} \right). \quad (17)$$

Here $p_A = -f_A + \mu_A n_A$, ($\mu_A = \partial f_A / \partial n_A$), etc. are the “intrinsic” pressures (chemical potentials) of each phase. The word “intrinsic” stands for the values of these quantities in the presence of a fictitious fully compensating background, in other words they refer to a uniform single-phase situation. Equations (16),(17) determine the jump in these quantities at the interface in order to have thermodynamic equilibrium when long range Coulomb forces and surface energy are present. These equations are valid for a general geometry described by the function $u(x)$. Notice that as long as $u(x)$ preserves the phase exchange symmetry the equations also preserve this symmetry.

To analyze the effect of the long range forces and of the surface energy in the jumps let us neglect for simplicity the density dependence of the surface energy ($\partial\sigma/\partial n_A = \partial\sigma/\partial n_B = 0$) and concentrate on the drop geometry. Due to the different charge distributions, the electrostatic potential energy $-e\phi$ of an electron inside and outside the drops is different. In equilibrium this jump in the electrostatic potential should be com-

pensated by a jump of the intrinsic chemical potentials [Eq. (16)] to make the electrochemical potential constant in the whole system. For $\delta > 0$ the drop repels electrons so the electrostatic potential energy will be lower outside the drop i.e. $-e\phi_A < -e\phi_B$. The intrinsic chemical potential outside will have to be larger than inside as the sign in Eq. (16) implies.

Regarding the pressure, in equilibrium the intrinsic pressure inside the drop, p_B , should equal the pressure exerted by the host p_A plus the pressure exerted by the mixing forces. For $\delta > 0$ the electrostatic energy induces a negative contribution to the pressure since an increase in the drop volume at constant particle number decreases the difference in densities between the interior and the exterior of the drop and hence the Coulomb cost. This effect is given by the first term in Eq. (17). The second term proportional to $u'(x)$ is a geometric contribution. Both terms are discussed in more detail in a specific example in Appendix B.

In the limit $e \rightarrow 0$ one gets $\mu_B = \mu_A = \mu$ and $p_A = p_B = p$ i.e. $\mu\delta = f_B - f_A$ which are the conditions for MC.

III. GENERAL ANALYSIS OF THE MIXED STATE IN THE UNIFORM DENSITY APPROXIMATION

In this section we set up the basic ideas for inhomogeneous solutions. For simplicity we model each phase free energy with a parabola and we assume that the surface tension is density independent. Without loss of generality we write the parabolas as a quadratic expansion around the MC densities:

$$f_A(n_A) = f_A^0 + \mu^0(n_A - n_A^0) + \frac{1}{2k_A}(n_A - n_A^0)^2 \quad (18)$$

$$f_B(n_B) = f_B^0 + \mu^0(n_B - n_B^0) + \frac{1}{2k_B}(n_B - n_B^0)^2$$

The quantities with the “0” superscript (or subscript below) satisfy MC in the absence of LRC forces i.e. $f_B^0 - f_A^0 = \mu^0\delta_0$ and $\delta_0 = n_B^0 - n_A^0$. The linear slope μ^0 is the same for the two phases due to the MC condition. The MC density n_0 and the volume fraction are related by $n_0 = n_A^0 + \delta_0 x$. The constants k_A, k_B are essentially the compressibilities of the two phases.¹²

For non interacting electrons at $T=0$ the compressibility coincide with the density of states. For the 3D free electron gas we have:

$$k_{free} = \frac{3^{1/3} m n_0^{1/3}}{\pi^{4/3} \hbar^2} \quad (19)$$

with m the electronic mass.

Another useful realization is a nondegenerate gas where we have:

$$k_{gas} = \frac{n_0}{KT} \quad (20)$$

Our aim in the following is to obtain the equations which control the deviation from MC behavior in the presence of the mixing energy.

We define a dimensionless global density

$$n' \equiv (n - n_A^0)/\delta_0$$

which measures the distance from the point in which B phase appears in the absence of Coulomb forces. In MC the coexistence region is given by $0 < n' < 1$.

Eqs. (16),(17) determine δ , and x for a fixed density where now μ_A, μ_B, p_A , and p_B can be expressed in terms of the parameters appearing in Eqs. (18).

In practice it is much easier to solve the equations by fixing the volume fraction x and solving for δ , and n , i.e. we find which density one should put in the system to obtain a mixed state with a given volume fraction. This is because the solutions happen to be multivalued functions of n whereas they are single valued functions of x (see below).

For a fixed volume fraction x we define the dimensionless density deviations from the MC values: $\hat{n} = (n - n_0)/\delta_0$ and $\hat{\delta} = (\delta - \delta_0)/\delta_0$. The density deviation \hat{n} measures the shift in the global density needed to have the same volume fraction of a system without LRC interaction.

To fix the energy units it is convenient to choose one of the two compressibilities as a reference, for example the largest. We define $k_m = \max(k_A, k_B)$. Energies per unit volume will be measured in units of the characteristic PS energy δ_0^2/k_m . The latter is essentially the difference between the uniform parabolic free energy and the MC free energy at the characteristic density δ_0 .

Now we define two important reference lengths scales in the theory. The characteristic size of an inhomogeneity for which the Coulomb energy balance the surface energy is given by the R_c of previous section with the geometric factors dropped and the density evaluated at the MC value. This define the scale

$$l_d = \left(\frac{\sigma \epsilon_0}{e^2 \delta_0^2} \right)^{1/3}. \quad (21)$$

The other length is given by $l_s^2 = \epsilon_0/(4\pi e^2 k_m)$. By relaxing the UDA we will show in section Sec. IV that l_s is a screening length. In other words if the reference phase (the one with k_m) is interpreted as a metal l_s is the characteristic distance in which the electric field penetrates.

The theory has two dimensionless parameters. One is the ratio k_B/k_A . The other measures the strength of the mixing energy effects in units of the characteristic PS energy δ_0^2/k_m and is given by:

$$\lambda = 2 \frac{k_m}{\delta_0^2} \left(\frac{9\pi e^2 \delta_0^2 \sigma^2}{5\epsilon_0} \right)^{1/3} = \frac{1}{2} \left(\frac{9}{5\pi^2} \right)^{1/3} \left(\frac{l_d}{l_s} \right)^2 \quad (22)$$

The characteristic mixing energy is given by the factor with the power $1/3$ in the middle expression. The constant λ characterizes the competition of the mixing energy cost and the MC like energy gain due to phase separation. The coupling constant goes to zero as $e \rightarrow 0$ with σ finite. This correspond to the usual PS. The case $\sigma \rightarrow 0$ with finite e correspond to an infinite number of drops (or layers) of zero radius. In this maximum intermixing situation the charges of the two phases spatially coincide and the Coulomb cost goes also to zero so that the MC is again valid. Notice however that this last idealized situation cannot be reached in practice because at some point for small drop radius the continuous approximation will fail.

Inserting the explicit expressions [Eqs. (18)] of f_A and f_B in Eqs. (16),(17) we obtain the following equations for the density deviations:

$$\hat{n} \left(\frac{1}{k_B} - \frac{1}{k_A} \right) + \hat{\delta} \left(\frac{1-x}{k_B} + \frac{x}{k_A} \right) = \left(\frac{5}{9\pi} \right)^{1/3} \frac{\lambda u(x)}{3k_m(1+\hat{\delta})^{1/3}x(1-x)} \quad (23)$$

$$\begin{aligned} \frac{x\hat{\delta} - \hat{n}}{k_A} + \left[\hat{n}\hat{\delta}(1-x) + \frac{\hat{n}^2}{2} \right] \left(\frac{1}{k_B} - \frac{1}{k_A} \right) + \frac{\hat{\delta}^2}{2} \left[\frac{1-2x}{k_B} + \frac{2x}{k_A} + \left(\frac{1}{k_B} - \frac{1}{k_A} \right) x^2 \right] = \\ \left(\frac{5}{9\pi} \right)^{1/3} \frac{\lambda(1+\hat{\delta})^{2/3}}{2k_m} \left[u'(x) + \frac{2u(x)}{3(1-x)} \right]. \end{aligned}$$

Eqs. (23) can be solved numerically for general values of the parameters. For small λ i.e. for small mixing energy we can linearize the equations neglecting higher order terms in $\hat{\delta}$ and \hat{n} . We will refer to this as the linearized UDA. We get:

$$\hat{n} \left(\frac{1}{k_B} - \frac{1}{k_A} \right) + \hat{\delta} \left(\frac{1-x}{k_B} + \frac{x}{k_A} \right) = \left(\frac{5}{9\pi} \right)^{1/3} \frac{\lambda u(x)}{3k_m x(1-x)} \quad (24)$$

$$\frac{x\hat{\delta} - \hat{n}}{k_A} = - \left(\frac{5}{9\pi} \right)^{1/3} \frac{\lambda}{2k_m} \left[u'(x) + \frac{2u(x)}{3(1-x)} \right] \quad (25)$$

For the sake of simplicity in the following we will consider the linearized solution. We checked that for all the physical properties the difference between the linearized and the exact solution is quite small in the range of λ where the drop solution is stable.

The linearized solution takes a simple form and is explicitly symmetric respect to an exchange of phases when written in the original variables:

$$n_A = n_A^0 + \frac{1}{6} \left(\frac{15}{\pi} \right)^{1/3} \frac{k_A}{k_m} \lambda \delta_0 \left[u'(x) + \frac{2u(x)}{3(1-x)} \right]$$

(26)

$$n_B = n_B^0 + \frac{1}{6} \left(\frac{15}{\pi} \right)^{1/3} \frac{k_B}{k_m} \lambda \delta_0 \left[u'(x) - \frac{2u(x)}{3x} \right].$$

In the case of $\lambda = 0$, according to MC, the system separates in two phases with densities n_A^0 , n_B^0 respectively independently of the volume fraction. For nonzero λ and small x the B phase divides in drops or layers and the density in each phase depends on the volume fraction of B phase. The deviation of each density from MC prediction is proportional to λ and to the compressibility of each phase. Notice that the density of an incompressible phase ($k \rightarrow 0$) does not depend on the volume fraction even in the presence of LRC forces.

In Fig. 3 we show the behavior of the two functions which determine the dependence of the densities on the volume fraction. In the drop geometry and for small x both n_A and n_B tend to be larger than in the MC case whereas in the layered geometry only n_A is larger. This gives rise to minor qualitative differences in the behavior of drops and layers. Apart from this the overall behavior is similar.

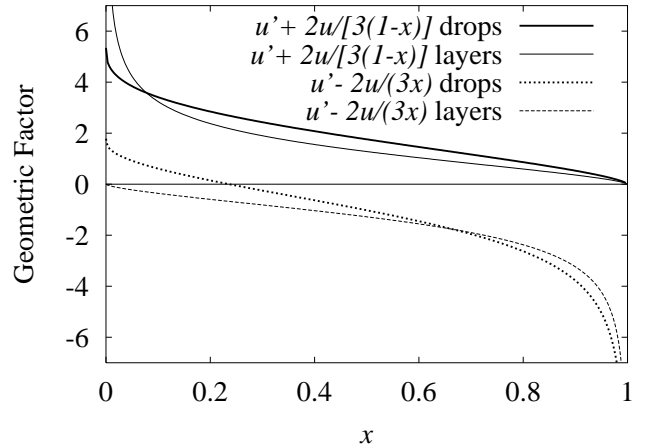


FIG. 3. The dimensionless functions that determine the change in n_A (upper curves) and n_B (lower curves) for small λ vs. the volume fraction x for the layered and the drop geometry. [See Eq. (26)]

The equation for the density of one phase [Eq. (26)] has a transparent interpretation in the limit in which the other phase, say A , is incompressible ($k_A = 0$). This case is solved in detail in Appendix B. Assume that A phase is the vacuum and so exerts no pressure and has zero density. We can consider that the mixing forces due to the electrostatic and surface energies exert an “external” pressure on the B phase inhomogeneity. In equilibrium the intrinsic pressure of B phase (p_B) should compensate this “mixing pressure” ($p_B = p_m$). The latter is shown in Appendix B to be given by:

$$p_m = \frac{\partial e_m}{\partial x} - \frac{2e_m}{3x} \quad (27)$$

On the other hand a change in the external pressure correspond to a change in the n_B density according to the B phase equation of state. This follows directly from our definition of compressibility:¹²

$$k_B \equiv n_B^0 \frac{\Delta n_B}{\Delta p_B}$$

where we have replaced a derivative by a finite different ratio. We can obtain the second linearized expression in Eq. (26) directly from this definition using that the MC density correspond to zero intrinsic pressure.

$$n_B - n_B^0 = k_B \frac{p_B}{n_B^0} \propto k_B n_B^0 \left[u'(x) - \frac{2u(x)}{3x} \right].$$

The mixing pressure can be negative as explained in the Appendix B. This implies that the density is less than the MC density. From the lower curves in Fig. 3 we see that for drops the pressure is positive for small x and then becomes negative whereas for layers the pressure is negative for all x .

Remarkably in both cases the mixing pressure is a decreasing function of x . Since in general x is an increasing function of n' we can anticipate that n_B will decrease as n' increase (see below). Notice that for small x we have $p_B \sim u'(x)/3$ so a decreasing mixing pressure can be directly related to the negative curvature of $u(x)$ (Fig. 2).

Coming back to the general solution in Eq. (26) we are interested in the dependence of these quantities as a function of the global density n' , our true control variable, rather than as a function of the volume fraction. Hence we need the volume fraction as a function of the global density n' . From the solution of the linearized equations we find:

$$n' = x + \left(\frac{15}{\pi} \right)^{1/3} \frac{\lambda}{6} x \quad (28)$$

$$\left(\frac{k_A(1-x)}{k_m} \left[u'(x) + \frac{2u(x)}{3(1-x)} \right] + \frac{k_B x}{k_m} \left[u'(x) - \frac{2u(x)}{3x} \right] \right)$$

Since all physical quantities depend on the densities this completes the solution of the problem.

Specific results will be presented in the next section for the drop geometry and in Sec. IV A for the layered geometry.

A. Results of the UDA for the drop geometry

Now we consider the drop geometry and we analyze in detail the two cases: i) the compressibilities of the two phases are equal ($k_B = k_A = k_m$) and ii) one of the compressibilities is zero.

In Fig. 4 we plot the volume fraction as a function of global density from Eq. (28) for the drop solution. The

volume fraction is a multivalued function of n' and in the case $k_B = k_A$ has a lower branch close to $x = 0$, an intermediate branch, and an upper branch close to $x = 1$. The intermediate branch is the physical solution. This will be shown below by looking at the free energy. The physical solution has the intuitive property that the volume fraction increases as global density increases.

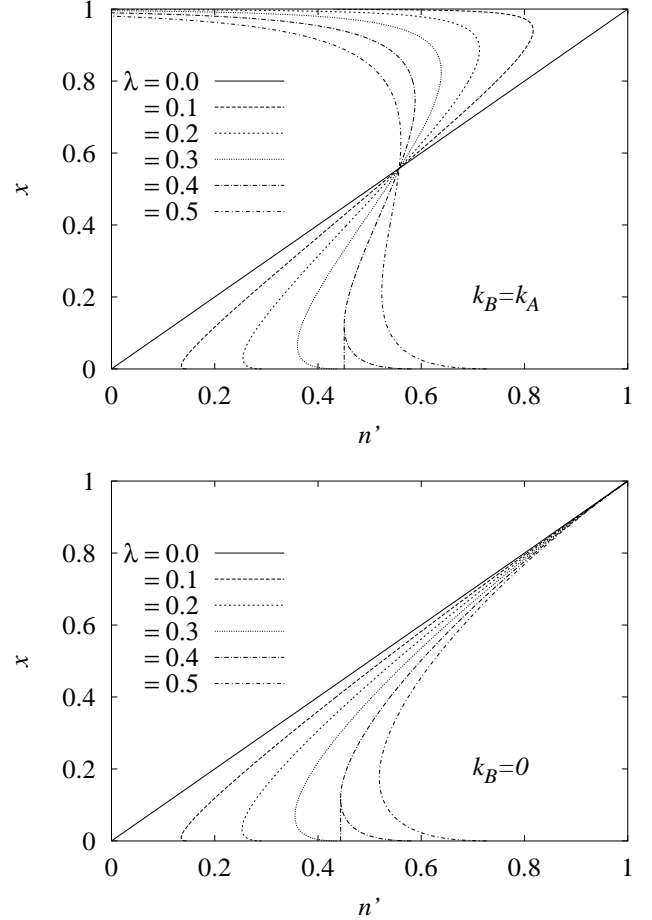


FIG. 4. Top panel: Volume fraction vs. n' for (from left to right at the bottom) $\lambda = 0, 0.1, 0.2, 0.3, 0.4, 0.5$ and $k_B = k_A$. For $\lambda = 0.4$ we indicate with a vertical line the discontinuity in the volume fraction to go from the uniform solution to the drop solution by increasing the density. Bottom panel: Same for $k_B = 0$. The approximations done are rigorously valid only for small x .

We see that the bifurcation density n'_{bif} at which the phase separated solution appears for finite λ is larger than in MC. On the other hand B phase appears with a finite volume fraction and its growing rate is larger than in the MC case. Remarkably both the volume fraction at the bifurcation point and the bifurcation density n'_{bif} are almost the same for $k_B = k_A$ and for $k_B = 0$. They depend only on λ as can be seen by comparing the two panels in Fig. 4.

In the case $k_B = 0$ the constraint between the volume

fraction and the densities together with the fact that the B density is fixed make all the curves to converge to the MC case when $x \rightarrow 1$ as shown in Fig. 4. The same happens when $k_A = 0$ and $x \rightarrow 0$.

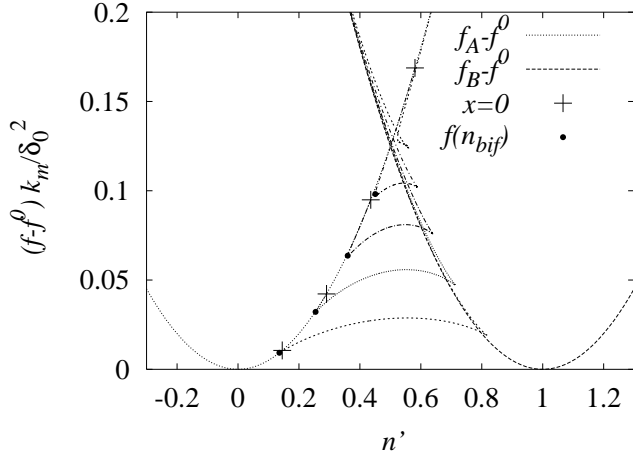


FIG. 5. $f_A - f^0$, $f_B - f^0$, and $f - f^0$ in the drop solution for $\lambda = 0.1, 0.2, 0.3, 0.4, 0.5$ (from bottom to top) and $k_B = k_A$ vs. n' . Here f^0 is the MC free energy for $\lambda = 0$ (a straight line). The cross indicates the value with $x = 0$ of the drop solution for each λ . The black dot indicates the bifurcation point in which the drop solution first appears when density increases.

To decide the stability of the solution we have to compare the drop solution with the single phase solution. In Fig. 5 we show $f_A(n')$, $f_B(n')$ and the total free energy with $k_B = k_A$ for various λ . The MC line $f^0(n') = f_A^0 + n'(f_B^0 - f_A^0)$ has been subtracted. The energy also is a multivalued function of n' . As the density increases the drop solution appears at n'_{bif} (indicated in Fig. 5 by a black dot) with two different branches. In the upper (unstable) branch x decreases with density till the point $x = 0$ highlighted with a cross in Fig. 5. For the lower branch one finds the expected behavior i.e. x increases with density. The upper branch is almost degenerate with the bulk $f_A(n)$ free energy. Near the bifurcation the three solutions (homogeneous, drop stable and drop unstable) are very close in energy. Approximation in the solution of the Eq. (23) can lead to wrong conclusions about the relative stability. In this case one has to refer to the non-linearized solution. For the latter (not shown) we find that the bifurcation density n_{bif} is lower than the density n_c at which the energy of the lower energy drop solution crosses the energy of the uniform phase $f_A(n')$. However the difference between n_c and n_{bif} is negligible for all practical purposes except for the largest λ . In this case there is a small region ($\lambda_c = 0.49 < \lambda < 0.57$) in which the lower energy drop solution still exist but is less stable than the homogeneous solution. If we neglect this small effect the phase diagram of the drop solution is

given by n_{bif} vs. λ as shown in Fig. 6. The uniform-drop boundary line is determined by the condition $\partial n'/\partial x = 0$ (see Fig. 4).

For $\lambda > \lambda_c$ the homogeneous solution is stable for any global density. The uniform A-B boundary line is determined by the crossings of the parabolas in Fig. 5.

When one of the compressibilities goes to zero, say k_B , the crossing moves to the right in Fig. 5 and the uniform B region shrinks until the boundary line for uniform B phase approaches the MC value ($n = n_B^0$). At the same time λ_c increases. Analogous results are obtain for k_A going to zero.

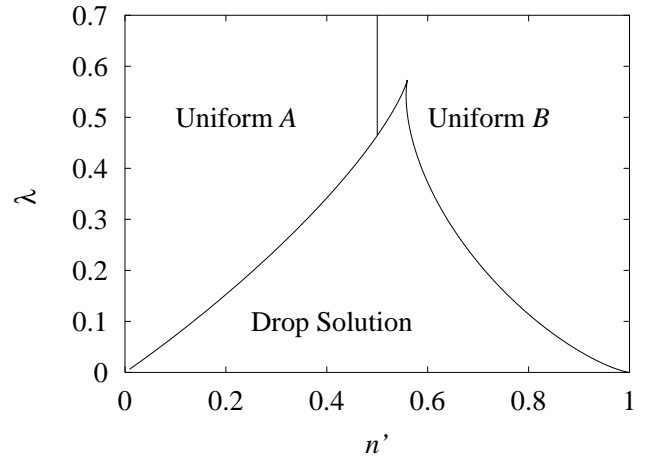


FIG. 6. Locus of existence of the low-energy drop solution in the λ - n' plane for $k_A = k_B$. This almost coincides with the phase diagram in the sense that when the drop solution exist it is more stable than the uniform solution except close to $\lambda = 0.5$ and in a very narrow region around the drop-uniform boundary line (see text).

In the upper panel of Fig. 7 we show the density of each phase as a function of the global densities for $k_B = k_A$. Increasing the global density the transition occurs from the uniform A phase, with density higher than the MC one, to the drop state. In the MC case the density of A phase is continuous at the transition and remains constant in the coexistence region. For nonzero λ the A density has a discontinuity when the drops occur (see inset). Remarkably both local densities decrease as the global density increases. This is due to the behavior of the mixing pressure as explained above and in Appendix B. In the case $k_A = 0$ the regions with $n_B > n_B^0$ ($n_B < n_B^0$) can be directly associated with positive (negative) mixing pressures.

Compared to the upper panel the lower curves for n_A shrink to the MC case and the upper curves for n_B remain very similar (even quantitatively) except close to $n' \rightarrow 0$. We mention that in the case $k_B = 0$ (not shown) a similar effect is seen exchanging A with B .

In Fig. 8 we show the cell radius and drop radius in

units of the screening length as a function of density for $k_B = k_A$. Both the cell and the drop radius are typically on the scale of a few screening lengths l_s for not too small λ and have a finite size at the appearance of the mixed state. The cell radius decreases as the density goes away from the bifurcation value to reach a minimum close to $n' = 1/2$. The minimum would be exactly at $n' = 1/2$ in an exact computation due to phase exchange symmetry. This is shown below in the layered solution.

The (B phase) drop radius instead is intrinsically asymmetric and increases monotonously with the density reflecting the transformation of the cell from A phase to B phase.

For $\lambda \rightarrow 0$ the cell radius and the drop radius behave as $R \sim \sqrt{\lambda} l_s \sim [\sigma \epsilon_0 / (\delta_0 e)^2]^{1/3}$. As stated in Sec. II they diverge as $e \rightarrow 0$ indicating that MC can be realized with a single large drop of B phase in A .

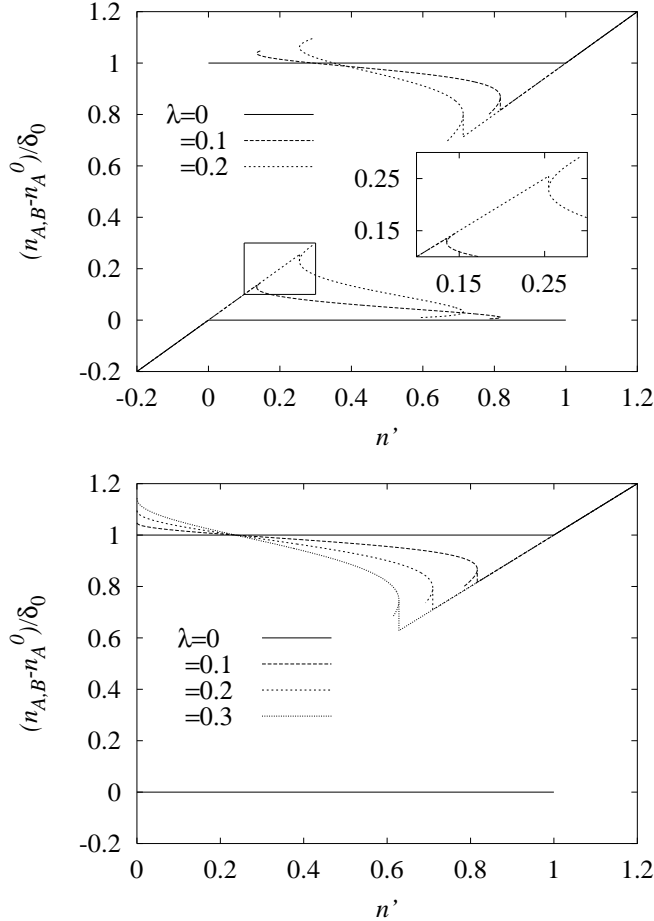


FIG. 7. Normalized densities of each phase as a function of normalized global density n' for different λ . The upper panel is for $k_B = k_A$ and the lower panel is for $k_A = 0$. For each panel the lower curves correspond to A phase and the upper curves to B phase. In the coexistence region multi-valued densities appear. The long branch is the physical one and the short branches are unphysical. The inset shows an enlargement of the A density to resolve the discontinuities.

Another peculiarity of the curves in Fig. 5 is that the free energy of the drop solution has the “wrong” curvature, that is the compressibility (defined from $\partial^2 f / \partial^2 n$) is negative. This does not necessarily imply an instability since the usual stability condition of positive compressibility is formulated for a neutral system, that is including the background compressibility. Since we are assuming the inverse background compressibility to be an infinite positive number (in our analysis the background density has a fixed homogeneous value) it follows that the total compressibility is positive and from this point of view the system is in a stable mixed state. Of course this does not guarantee stability against more complicated solutions than the simple crystal of drops.

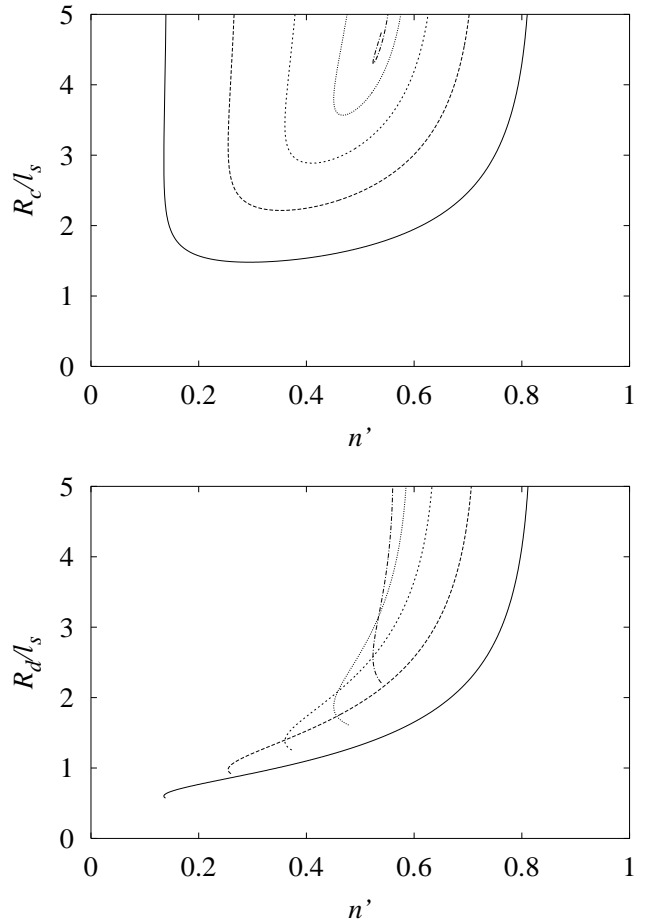


FIG. 8. R_c and R_d in units of the screening length l_s defined above Eq. (22) vs. n' for $k_B = k_A$. We show the curves for $\lambda = 0.1, 0.2, 0.3, 0.4, 0.5$ which increases from bottom to top in the top panel and from right to left at the top in the lower panel. In the top (bottom) panel for each curve the lower (upper) branch is the stable one.

The situation is more severe for $\lambda > \lambda_c$ where the drop solution, if it exists, is not stable. In this case, the system remains always single phase and the free energy is given by the branches of the parabola with the smaller

energy in Fig. 5. It changes suddenly from A phase to B phase at the density n'_c for which $f_A(n'_c) = f_B(n'_c)$. (For our parameters $n'_c = 0.5$). The problem is now that the energy has a cusp pointing upwards at n'_c which implies an infinite negative inverse compressibility. This will compete with the infinite positive inverse compressibility of the background. Clearly one should consider in this case the background compressibility (e.g. the lattice compressibility) since the beginning. As a first step we can add to the above electronic free energy a background free energy contribution $f_b(n) = (n - n_c)^2/2k_b$. A very rigid (but not infinitely rigid) background is described by a very small $k_b > 0$ which correspond to a very narrow parabola for the background free energy. The total free energy, background plus cusp, will have a cusp pointing up with two local minima nearby. Since now the total free energy corresponds to a truly neutral system one can make a MC between the two local minima. One obtains a phase separation between A and B with the background adjusting its density in each region to the density of each phase to make it neutral. The same argument applies at the critical density where the drop solution crosses the uniform solution, although the negative dip is much less pronounced in that case. Usually the electronic system is a crystal where the background is provided by the ionic lattice. If one trays to prepare the crystal with an electronic density close to the critical one the system can break in two pieces each one with a different lattice constant. Typically the crystal is not at a fixed volume but at a fixed external pressure P . (We use capital P to distinguish the pressure exerted on the crystal as a whole from the electronic pressures of the phases p_A and p_B). In this situation MC determines the equilibrium pressure P_0 for phase coexistence. P_0 will depend on the global doping so above λ_c , P_0 vs. doping determines a phase boundary line which will cut ambient pressure at some critical doping.

Since the electronic free energies depend on external parameters, a remarkable implication is that the critical doping will also depend on external parameters like magnetic field, temperature, pressure, etc. In other words a crystal can be driven from a single phase to a two phase situation by changing external parameters. This is very reminiscent of the situation in some manganites where one finds that a single phase crystal brakes in a multidomain crystal by lowering the temperature. The multidomain system shows lattice mismatch and large stress at the interfaces.^{13,14}

In Sec. IV A analogous results are presented for the layered geometry case and compared with a more elaborate computation which relax the UDA. In paper II we apply to different physical systems the ideas developed in this section.

IV. LOCAL DENSITY APPROXIMATION

In this section we generalize our results to take into account the full spatial dependence of the density. The basic assumption is that we can write the free energy of each phase as the spatial integral of a free energy density which is a function of the local density. i.e. we are using a local density approximation (LDA). The free energy reads:

$$F = \int_{\mathbf{r} \in A} d^3\mathbf{r} f_A[n(\mathbf{r})] + \int_{\mathbf{r} \in B} d^3\mathbf{r} f_B[n(\mathbf{r})] + \frac{1}{8\pi} \int d^3\mathbf{r} \mathbf{E}^2 + S_{AB}\sigma \quad (29)$$

Here $\mathbf{r} \in A$ indicates that the integral is restricted to the regions of phase A and S_{AB} is the total interface surface between A and B and we assume for simplicity $\epsilon_0 = 1$. One should be careful not to double count in σ surface energy costs that are due to the spatial variation of the charge since this will be explicitly taken into account in the first three terms. On the other hand one can include in σ other effects, like magnetic, which would not be included otherwise. For simplicity we will assume σ to be density independent.

The electric field is related to the total charge density (electronic plus background) through Poisson equation:

$$\nabla \cdot \mathbf{E} = 4\pi\rho \quad (30)$$

with the total charge density:

$$\rho = -e[n(\mathbf{r}) - \bar{n}] \quad (31)$$

Here \bar{n} is the global density of the previous section and the bar distinguishes it from the spatially varying density $n(\mathbf{r})$. Notice that $e\bar{n}$ is the charge density of the background. The condition of neutrality is written as:

$$\bar{n} = \frac{1}{V} \int_{\mathbf{r} \in A} d^3\mathbf{r} n(\mathbf{r}) + \frac{1}{V} \int_{\mathbf{r} \in B} d^3\mathbf{r} n(\mathbf{r}) \quad (32)$$

Using $n(\mathbf{r}) = n_A$ for $\mathbf{r} \in A$ and $n(\mathbf{r}) = n_B$ for $\mathbf{r} \in B$ one recovers the UDA.

Instead of minimizing the functional with respect to the density it is convenient to use Eqs. (30),(31) to express the density as a function of the electric field, $[n = n(\nabla \cdot \mathbf{E})]$ and minimize the functional with respect to the electric field profile. We look for periodic solutions (layer, crystal, etc) and restrict the computation to one cell.

Minimizing the free energy [Eq. (29)] respect to the electric field one obtains:

$$\mathbf{E} = -\frac{1}{e} \nabla \frac{\partial f_X}{\partial n} [n(\nabla \cdot \mathbf{E})] \quad (33)$$

where $X = A$ or B when $\mathbf{r} \in A$ or $\mathbf{r} \in B$ respectively. This differential equation together with the boundary

condition determines the field profile. The boundary condition at the cell boundary and at the internal boundary will be discussed in the example below. Once the electric field profile is known for a given geometry the density profile is given by Poisson equation. As a final step one should optimize the geometry.

Introducing the parabolic expressions [Eqs. (18)] to parameterize the free energy densities in Eq. (33) one obtains:

$$\mathbf{E} = l_X^2 \nabla \nabla \cdot \mathbf{E} \quad (34)$$

with $l_X^2 = (4\pi e^2 k_X)^{-1}$. Clearly l_X is the screening length as anticipated in Sec. III. If we use the compressibility of a free electron gas for k_X [Eq. 19] and reintroduce the dielectric constant l_X corresponds to the Thomas-Fermi screening length:

$$l_X^2 = \left(\frac{\pi}{3}\right)^{1/3} \frac{\epsilon_0 \hbar^2}{4e^2 m (n_X^0)^{1/3}}. \quad (35)$$

We reach Thomas-Fermi theory which is the simplest version of the LDA used for electronic structure computations. If we use the nondegenerate gas compressibility [Eq. (20)] l_X is the Debye-Hückel screening length.

A. Solution for the layered geometry

In the layered geometry the differential Eq. (34) reduces to a one-dimensional problem and can be readily solved. The geometry is identical as in the UDA approximation (Fig. 1). The central B layer has width $2R_d$ and the cell has width $2R_c$. The r coordinate is perpendicular to the layers and $r = 0$ corresponds to the center of the B layer. By symmetry the field is zero at $r = 0$ and $r = R_c$. In this case the boundary condition $\mathbf{E}_\perp = 0$ for the electric field perpendicular to the surface at the cell boundary automatically warrants the neutrality condition [Eq. (32)] due to Gauss theorem.

Apart from the cell boundary the cell itself has an internal boundary that divides A and B phases we call E_0 the electric field at the A - B boundary. The value of E_0 is also optimized and this provides an additional boundary condition.

The solution is of the form:

$$E_A(r) = E_0 \frac{\sinh[(r - R_c)/l_A]}{\sinh[(R_d - R_c)/l_A]} \quad (36)$$

$$E_B(r) = E_0 \frac{\sinh(r/l_B)}{\sinh(R_d/l_B)}$$

where $E_A(r) \equiv E(r)$ for $r \in A$, etc.

The charge density is given by:

$$\rho_A = \frac{E_0}{4\pi l_A} \frac{\cosh[(r - R_c)/l_A]}{\sinh[(R_d - R_c)/l_A]}$$

(37)

$$\rho_B = \frac{E_0}{4\pi l_B} \frac{\cosh(r/l_B)}{\sinh(R_d/l_B)}$$

The electric field at the A - B boundary can be related to the jump in the density at the interface:

$$E_0 = \frac{-4\pi e[n_B(R_d) - n_A(R_d)]}{[l_B \tanh(R_d/l_B)]^{-1} + \{l_A \tanh[(R_c - R_d)/l_A]\}^{-1}} \quad (38)$$

It plays the same role as the parameter δ in Sec. II so that we can find the optimum charge distribution between A and B by minimizing the free energy with respect to E_0 .

After replacing Eqs. (37),(38) in the expression for the free energy [Eq. (29)] and minimizing respect to E_0 we find:

$$E_0 = \frac{4\pi e \delta_0 [l_B^2 (n' - 1) - l_A^2 n']}{l_B / \tanh(x R_c / l_B) + l_A / \tanh[(1 - x) / l_B]} \quad (39)$$

where δ_0 and n' are defined as in Sec. III and R_d has been eliminated in favor of the volume fraction with $R_d = x R_c$.

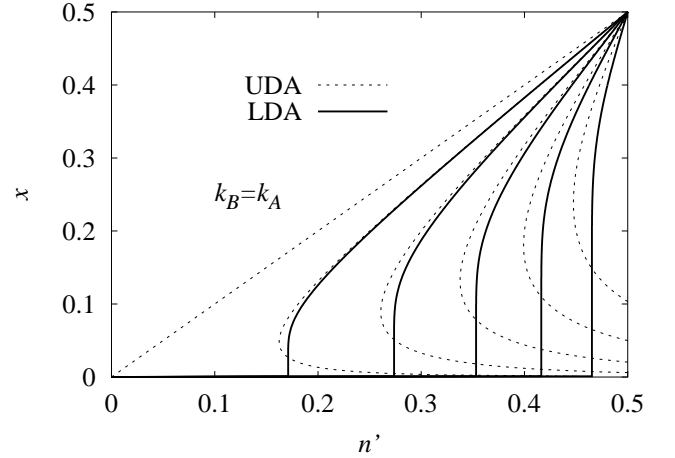


FIG. 9. Volume fraction vs. n' for (from left to right at the bottom) $\lambda = 0, 0.1, 0.2, 0.3, 0.4, 0.5$ and $k_B = k_A$ in the LDA (thick line) and the UDA (thin line). Only the lower left corner of the plot is shown since the upper right corner is symmetric by phase exchange. For the UDA approximation the lower branch is unphysical like in Sec. III A

At this point the total free energy per unit volume $f \equiv F/V$ takes the form:

$$f = f_A^0 + \delta_0 \mu_0 n' + \frac{\sigma}{R_c} + \frac{2\pi e^2 \delta_0^2 [l_A^2 (n')^2 (1 - x) + l_B^2 x (1 - n')^2]}{2\pi \delta_0^2 e^2 [-l_B^2 (1 - n') - l_A^2 n']^2} - \frac{2\pi \delta_0^2 e^2 [-l_B^2 (1 - n') - l_A^2 n']^2}{R_c \{l_B / \tanh(x R_c / l_B) + l_A / \tanh[(1 - x) R_c / l_A]\}} \quad (40)$$

The first two terms are the MC free energy, the third term is the surface energy and the last two terms are both contributions due to the shift from the MC densities and due to the electrostatic energy.

The last step is to minimize this free energy with respect to the volume fraction and R_c . This gives two equations which can be solved numerically for R_c and x . As in Sec. III it is easier to fix x and solve for R_c and n' .

In the following we present results for the case $k_B = k_A$ and compare with the linearized UDA of Sec. III for the layered geometry.

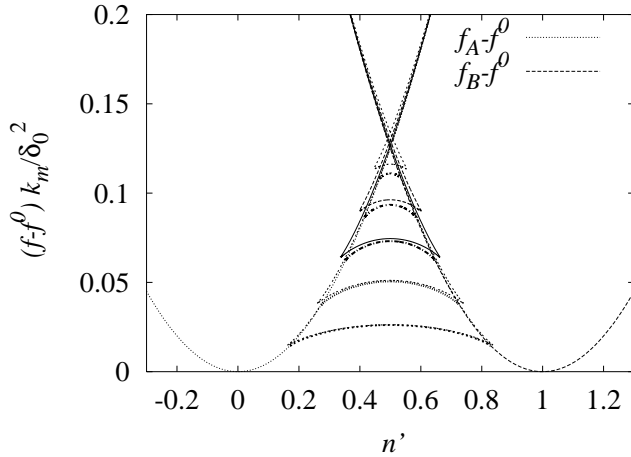


FIG. 10. $f_A - f^0$, $f_B - f^0$, and $f - f^0$ in the layered solution for $\lambda = 0.1, 0.2, 0.3, 0.4, 0.5$ (from bottom to top) and $k_B = k_A$ vs. n' in the LDA (thick line) and the UDA (thin line). Here f^0 is the MC free energy for $\lambda = 0$ (a straight line).

In Fig. 9 we plot the volume fraction as a function of global density in the LDA approximation and the UDA approximation. Clearly the results are very similar even quantitatively. In the UDA there is a jump on the volume fraction from zero to a finite value. In the LDA the volume fraction is not discontinuous but grows very rapidly at the threshold for the appearance of the inhomogeneous state. Another important difference is that the solutions are not any more multivalued in the LDA.

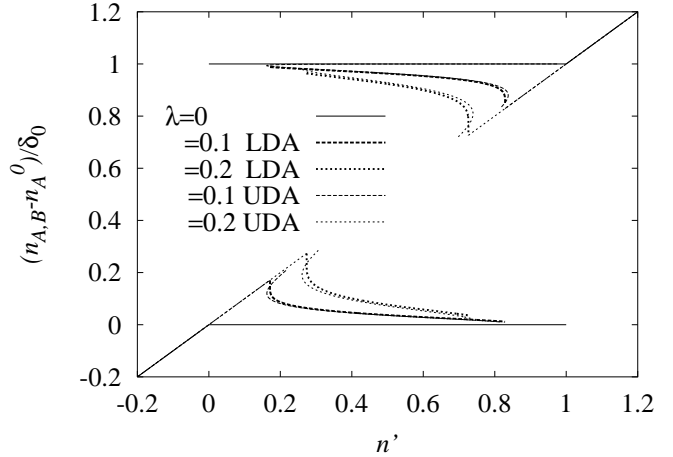


FIG. 11. Normalized spatially averaged densities of each phase as a function of normalized global density n' for different λ , $k_B = k_A$ and the linearized UDA (thin lines) and the LDA (thick lines). The lower curves correspond to A phase and the upper curves to B phase. In the coexistence region multivalued densities appear in the linearized UDA. The long branch is the physical one.

In Fig. 10 we show $f_A(n')$, $f_B(n')$ and the total free energy with $k_B = k_A$ for various λ . The MC line $f^0(n') = f_A^0 + n'(f_B^0 - f_A^0)$ has been subtracted. The behavior of the layered solution in the UDA is similar to the one found for drops in Sec. III A and coincides with it at small λ . In the LDA approximation multivaluation disappears. The relaxation of the UDA approximation produces obviously a gain in energy since the functional that we are minimizing is the same in LDA and the UDA but in the UDA we are imposing an extra constrain on the densities. The gain in energy however is quite small. The phase diagram in the UDA and the LDA (not shown) are both very similar (even quantitatively) to the one for drops of Sec. III A except that they are fully symmetric. The critical λ above which the inhomogeneous solution is never stable is given for $k_B = k_A$ by $\lambda_c = (9/5)^{1/3}/2 \sim 0.61$ in the LDA and by $\lambda_c \sim 0.70$ in the UDA.

In Fig. 11 we show the densities in each phase in the UDA. This is compared with the densities of each phase in the LDA averaged spatially over the space spanned by each phase. Again the behavior is remarkably similar and the density discontinuities of the UDA become very steep changes with LDA.

Finally in Fig. 12 we show the behavior of the dimensions of the cell and of the B layer as a function of global density. Due to perfect phase exchange symmetry the cell width $2R_c$ as a function of n' is symmetric and has the minimum exactly at $n' = 0.5$. The discontinuous jump at the threshold in the UDA becomes a divergence in the LDA. For the same parameters the cell width are smaller in the UDA than in the LDA. This can be understood by noticing that in the UDA the widths are of

order $l_s = [\sigma/(\delta_0 e)^2]^{1/3}$. Roughly speaking we can say that the effect of the LDA is: i) to increase the surface energy due to the bending of the charge distributions at the surface and ii) to screen the electric fields which can be schematized as an effective reduction of the charge e . Both effects tend to increase the width of the layers as found.

For small λ Fig. 12 shows that the LDA and UDA radius coincide just as the full solution. This is because $l_d \sim \sqrt{\lambda} l_s \ll l_s$ [c.f. Eqs. (21),(22)] so that the density is almost constant inside the layer even in the LDA and the solutions are virtually the same. In this case the Thomas-Fermi approximation is ineffective to generate a surface energy since all surface energy effects other than the ones explicitly included in σ are due to density variations. In other words if one sets $\sigma = 0$ the system prefers to make small drops to avoid both the Thomas-Fermi induced surface energy effect and the Coulomb cost. This however is a drawback of the Thomas-Fermi approximation since small drops will certainly have a large surface energy due to the confinement of the electron gas. It is well known that Thomas-Fermi theory is a poor approximation to model surfaces.¹⁵

If one increases λ inhomogeneities are possible until the point in which $l_d \sim l_s$ and $\lambda = \lambda_c$. It is not possible to have inhomogeneities of dimension $l_d \gg l_s$ because in the region far from the surface screening makes the local density to coincide with the global density and this inhibits any PS energy gain. It is then convenient for the system to avoid any surface and remain single phase.

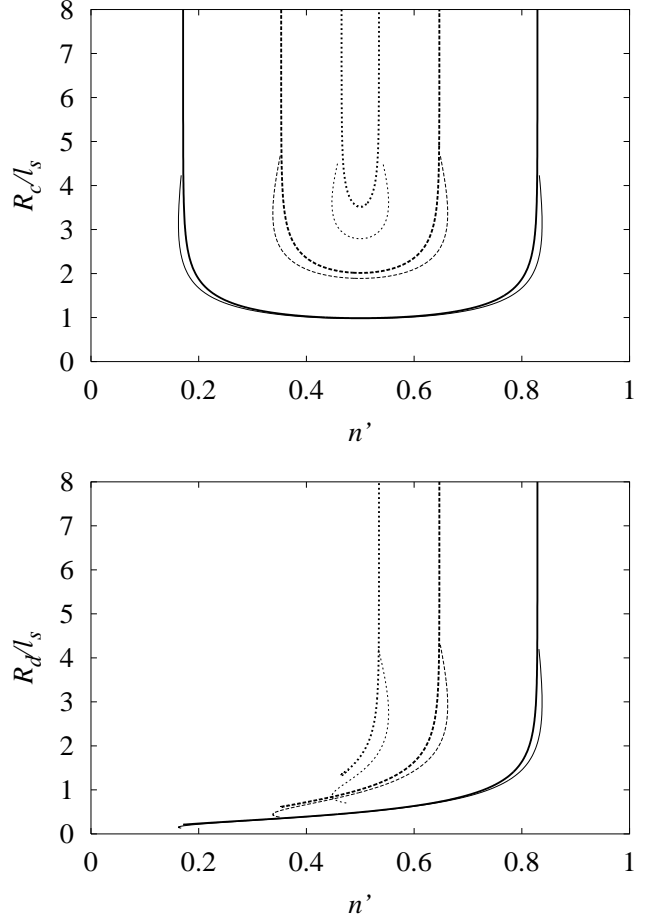


FIG. 12. R_c and R_d in units of the screening length l_s defined above Eq. (22) vs. n' in the linearized UDA (thin lines) and the LDA (thick lines). We show the curves for $\lambda = 0.1, 0.3, 0.5$ which increases from bottom to top in the top panel and from right to left at the top in the lower panel.

In Fig. 13 we show the density profile for $\lambda = 0.3$ and for two different values of the global density. One is close to the threshold for the appearance of B phase ($n' = 0.353$). In this case the A density is close to the density of the background and bends down close to the interface to screen the B layer charge. Well in the bulk of A phase, where the charge density coincides with the density of the background, we have $E \sim 0$ as expected for a metal. When the global density increases the local densities decrease according to the behavior discussed before for the average densities (Fig. 11). The layers become of the order of the screening length and the electric field is never completely screened.

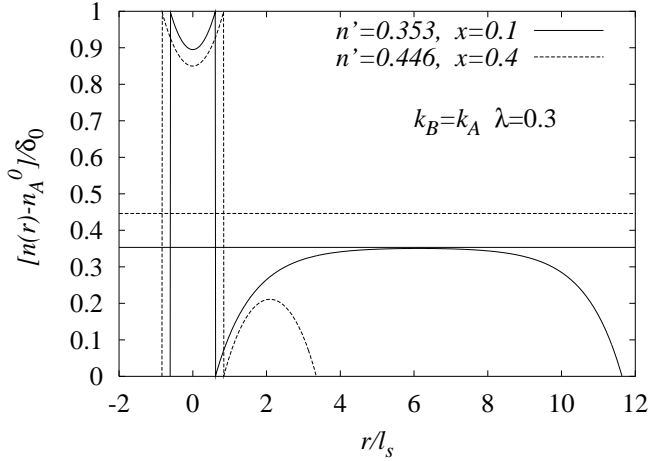


FIG. 13. Density profile for $\lambda = 0.3$ and different values of the global density. The region close to $r = 0$ corresponds to B phase and the rest is A phase. The structure repeats periodically in the r direction. The horizontal lines signal the global density.

V. CONCLUSIONS

In this work we have generalized the Maxwell construction to a situation that appears often in strongly correlated electronic systems, i.e. phase separation frustrated by the LRC interaction.

We discussed i) the stabilization of the uniform phases as the frustrating forces are increased, ii) the anomalous behavior of the frustrated phase separated mesoscopic state and iii) the singular behavior which results in a lattice instability when frustration dominates.

We used a UDA and a more involved LDA approach. Both are shown to give very similar results thus justifying in general the use of the much simpler UDA. For the LDA we have approximated the energy functional in the case of a metal with the the simplest LDA functional i.e. the Thomas-Fermi approximation. Our formulation however is general and allows for more sophisticated functionals.

As it is intuitively expected, the LRC interaction tends to stabilize the non-separated uniform phases in the presence of a rigid background. This has been illustrated in the general analysis of two generic phases described by parabolic free energies. We have shown that the region of phase separation contracts when the LRC and surface energy effects are switched on and disappears above a critical value of a dimensionless parameter λ . This parameter plays the role of an effective coupling and characterizes the competition between the energy cost due to the surface and Culombic energy and the energy gain in the MC i.e. it controls the degree of frustration. The balance between these energies determine whether the phase separated state exists or not.

When λ is small ($\lambda < \lambda_c$) a mixed state arises. We have modeled this situation by considering a Wigner crystal of drops of one phase hosted by the other phase and a layered geometry which behaves as one dimensional analog of the Wigner crystal. We believe that our general conclusions (including the existence of a critical λ) are not sensitive to the geometry of the mixed state as long as the two length scales R_c and R_d are present and both are much larger than the interparticle distance. The former length (cell size) characterizes a periodic structure and the latter (bubble size) how this periodic structure is divided to host the two phases. An indication that the geometry is not very important comes from the fact that the plots of the physical quantities in Sec. III for $k_A = k_B$ are quite symmetric to an exchange of the two phases, each one having a different shape. This means that the behavior of the drops is not much different from the behavior of their counterpart, the interstitial regions. The same happens when comparing the behavior of drops and layers.

In the mixed state novel non-linear effects appear which are not present in the unfrustrated MC. Within the UDA the volume fraction and the drop radius of the minority phase do not start from zero but from a finite value and the transition to the drops state is abrupt. In the LDA physical quantities are not discontinuous but grow very steep at the threshold mimicking the discontinuous behavior.

A further non-linear effect in the drop state is that the local densities of each phase have an anomalous behavior decreasing as the global density increases. This can affect properties of the system which are sensitive to the local density and will be illustrated in paper II with the Curie temperature of the manganites. We emphasize that also local probes like NMR, core spectroscopy etc. should be sensitive to this effect and may be used to detect Coulomb frustrated phase separation in real systems.

In the case of strong Coulomb interaction and large surface energy ($\lambda > \lambda_c$) a transition between two uniform phases occurs. We have shown that in this case the compressibility is singular and a lattice instability will take place if the ionic background is not fully rigid. The system (both electrons and ions) can separate in two neutral phases with different specific volumes.

In principle also at the transition point to the drop state a lattice instability can arise for the same reasons discussed in the $\lambda > \lambda_c$ case, although the instability is now much weaker.

When do we expect such a mesoscopic phase separation to prevail against microscopic phase separation (like stripes)? In order to have mesoscopic phase separation we need that the interparticle distance ($\sim n^{-1/3}$) be smaller than the inhomogeneous length l_d which should be smaller than the screening length l_s . This implies:

$$n^{-1/3} < \left(\frac{\sigma \epsilon_0}{e^2 \delta_0^2} \right)^{1/3} < \left(\frac{\epsilon_0}{4\pi e^2 k_m} \right)^{1/2}$$

We see that large dielectric constants favor both large drops and inhomogeneous states so polar materials which have typically large static dielectric constants ($\epsilon_0 \sim 10 \sim 100$) are ideal candidates. Small δ_0 or large σ favors large drops but a too small δ_0 or a too large σ can inhibit phase separation at all. Small values of δ_0 can occur in manganites where typically a variety of different ground states with close densities compete with each other (see paper II for a specific example). This suggests either large drops or total frustration with lattice instabilities close to the transition from one phase to the other. We mention that these lattice instabilities, which also involve volume variations, are reminiscent of the macroscopic phase separation observed in some manganites.¹³

Finally small compressibilities favor the PS states. This suggests that these effects can be important for bad metals or close to metal insulator transitions.

We believe that to some extent at least some of the effects found here can survive also in the microscopic frustrated phase separation. In fact for example, the corrections to the electrostatic energy due to the discreteness of the charge which are computed in the Appendix A for the very unfavorable case of a classical Wigner crystal can be irrelevant for small metallic inhomogeneities due to quantum blurring. In this case however one should take into account the structure of the underlying atomic potential. Of course if quantum blurring effects are too strong one should be concerned with the stability of the whole superstructure against quantum fluctuations.

APPENDIX A: CORRECTION DUE TO DISCRETENESS OF THE CHARGE

In order to compute the electrostatic energy in the UDA [Eq. (7)] we assume that the charge within one drop is spread uniformly. Variations of density can arise because of screening effects as discussed in Sec. IV A and because of intrinsic charge inhomogeneities internal to the particular phase. Here we discuss the latter effect.

Let us now consider an extreme limit and assume that both phases A and B are two classical Wigner crystals of electrons as a prototypical case in which the charge is intrinsically non-uniform. What is the correction to the Eq. (7)?

In the host phase we neglected the interaction between the neutral A Wigner crystal of electrons and a background of charge density $(n - n_A)e$ (see Fig. 1). The fluctuation of the charge inside the crystalline Wigner-Seitz cell can make this interaction nonzero. Also for the phase forming the drop we have to consider the interaction between the neutral B Wigner crystal and a background of charge density $(n - n_B)e$.

The electrostatic contribution per drop is:

$$\epsilon_{A-B} = -\frac{3eq_A}{10r_A}N_A$$

with

$$q_A = \frac{4\pi}{3}r_A^3(n - n_A)e$$

and a similar expressions for B phase. Here $\frac{4\pi}{3}r_A^3 = 1/n_A$ and N_A is the number of electrons of A phase in a drop:

$$N_A = n_A v_d \left(\frac{1}{x} - 1\right)$$

$$N_B = n_B v_d$$

The total contribution per unit volume to the electrostatic energy is:

$$\Delta e_e = \frac{2\pi e^2}{5}[(n_B - n)n_B r_B^2 x + (n_A - n)n_A r_A^2 (1 - x)] \quad (A1)$$

Clearly [c.f. Eq. (7)] the correction $\Delta e_e/e_e$ is of order $r_{A,B}^2/R_d^2$ so it is negligible unless the volume of the drop is of the order of the volume per particle in which case the whole computation has no sense.

APPENDIX B: “METALLIC” DROPS IN “VACUUM”

In this appendix we discuss in detail the case of a compressible phase (B) growing in an incompressible phase ($k_A = 0$). This simplifies the physics because the A density is fixed so there is no interchange of particles and the B density is not any more bivaluated for small densities as shown in the lower panel of Fig. 7. We present an alternative treatment of the frustrated phase separation phenomena which enlightens the underlying physics and discuss the pressure exerted by the mixing forces in detail.

To fix ideas we call B phase a “metal” and A phase the “vacuum”. Accordingly we put $n_A = n_A^0 = 0$ and $f_A = 0$. These last conditions do not change the solution but make the interpretation more transparent.

Since in this case the number of particles in each phase is fixed (zero for the vacuum) we can minimize the energy per particle $E \equiv f/n$ given by:

$$E = \frac{f_B}{n_B} + \frac{e_m(x, n_B)}{n} \quad (B1)$$

This has to be minimized respect to the volume fraction taking into account that the density n_B is also a function of the volume fraction given by the constrain $n_B = n/x$. By putting the derivative respect to x of Eq. (B1) equal to zero we obtain:

$$p_B = \frac{\partial e_m}{\partial x} - \frac{2}{3} \frac{e_m}{x} \quad (B2)$$

The left hand side originates in the first term in Eq. (B1) and is the intrinsic pressures of the metal, i.e the pressure

that the metal exerts on the surface. The right hand side is the pressure that the mixing forces, considered as “external” to the inhomogeneity, exert on the metal. We call this the mixing pressure (p_m). In equilibrium both pressures balance ($p_B = p_m$).

The mixing pressure has two terms, the first [right hand side of Eq. (B2)] comes from the explicit dependence of the mixing energy on the volume fraction at constant n_B and is proportional to $u'(x)$. For an ideally symmetric $u(x)$ (see Fig. 2) this term is positive for $x < 0$ and is negative for $x > 0$. We can say that this term tends to “compress” the metal in a less than half filled cell whereas it tends to “stretch” the metal (negative pressure) in the opposite case. This is just the expected tendency of the mixing energy to favor the closest uniform phase ($x = 1$ or $x = 0$). The second term is due to the dependence of the mixing energy on the volume fraction through n_B at constant particle number. An expansion of the cell at constant particle number produces a decrease on n_B which reduces the mixing energy [Eq. (13)]. This produces a negative pressure contribution proportional to $-u(x)/x$. The net contribution is given by $u'(x) - 2u(x)/(3x)$ [Eq. (B2)]. It follows that for more than half filled cells the metal is subject to a net negative pressure and for less than half filled cells the metal is subject to negative or positive pressures depending on the geometry and the volume fraction. The upper curves in Fig. 3 are proportional to $u'(x) - 2u(x)/(3x) - 1$. For drops the mixing pressure is positive for small x and then becomes negative whereas for layers the mixing pressure is negative for all x .

The appearance of negative pressures indicates that the metal can be stable at densities which in the absence of LRC forces would be unstable so it is an indication of the stabilization effect of the LRC forces. In Fig. 14 we show $E(n_B)$ for a parabolic free energy. The intrinsic pressure ($\propto dE/dn_B$) is negative for $n_B < n_B^0$ and is positive for $n_B > n_B^0$. We will show below that stable solutions can be found in the region $n_B < n_B^0$ which are inaccessible (unstable) according to MC.

The following example clarifies the physical meaning of the negative pressures. Consider a neutral liquid with short range attractive forces. At negative pressure molecules will be at distances larger than the equilibrium distance and this implies an energy cost proportional to the volume. The system can relax by creating a surface and relaxing all molecules to the equilibrium distance. The energy cost proportional to the surface is much less than the energy gain proportional to the volume and this produces the MC instability. In the presence of mesoscopic frustrated PS this can not be done because for the drops the surface is not any more negligible respect to the volume. In fact the optimum drop ratio can be seen as the length scale at which successively breaking large drops subject to the negative mixing pressure is not any more convenient due to the surface energy cost.

In the following we illustrate the behavior of the solution performing a graphical minimization of the en-

ergy for the drop geometry and the parabolic free energy Eq. (18). Instead of minimizing with respect to the volume fraction we use the constraint to eliminate the volume fraction in favor of n_B ($x = n/n_B$). The energy per unit particle is given by:

$$E - \mu^0 = \frac{n_0^B}{k_m} \left\{ \frac{(n_B - n_B^0)^2}{2n_B n_B^0} + \frac{3}{2^{4/3}} \lambda \left(\frac{n_0^B}{n_B} \right)^{1/3} \left[2 - 3 \left(\frac{n}{n_B} \right)^{1/3} + \frac{n}{n_B} \right]^{1/3} \right\} \quad (\text{B3})$$

The f_0^B term has been eliminated with the MC condition. The first term in the curly brackets is the bulk energy contribution. The mixing energy per particle is $e_m/(xn_B) \sim u(x)/(xn_B^{1/3})$ and contributes to the last term in the curly brackets. The geometric factor $u(x)/x$ gives the term in the square brackets.

The equilibrium density is found by minimizing Eq. (B3) with respect to n_B . In Fig. 14 we show $E - \mu^0$ as a function of n_B for $\lambda = 0.3$ and different values of n' . The thick line is the energy of the uniform metal [the first term in the brackets in Eq. (B3)] and is minimized at the MC density n_B^0 .

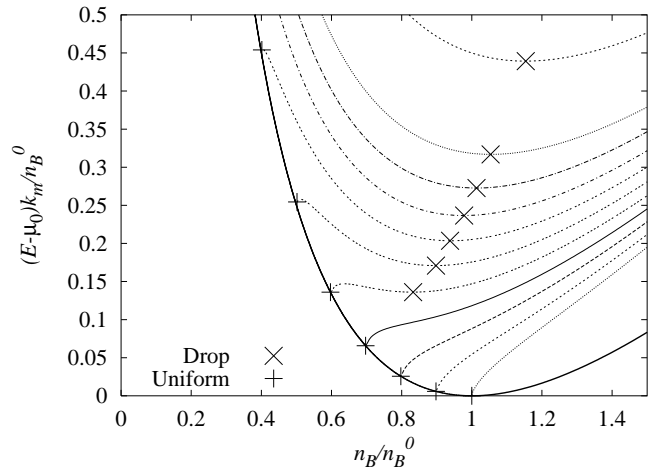


FIG. 14. Normalized energy per particle as a function of n_B/n_B^0 for $\lambda = 0.3$. The thick line corresponds to the uniform phase and the thin lines to the drop state with n' changing from zero (top) to one (bottom) in steps of 0.1. The crosses indicate the drop solution and the uniform solution.

For very small n (or x) the geometric factor is constant and the mixing energy contribution goes as $1/n_B^{1/3}$. This shifts the minimum to values of the density larger than n_B^0 as can be seen from the upper curves of Fig. 14 where the energy per particle is given for various values of the global density and $\lambda = 0.3$. This is due to the positive pressure exerted by the mixing energy of drops at small volume fraction and explains the behavior of the

n_B density in the limit $n' \rightarrow 0$ (Fig. 7). As the density increases the density dependence of the geometric factor tends to reduce the minimum to lower densities.

As a by product this computation illustrates the stabilization of a uniform solution by the long range interaction and the first order like nature of the transition. Above $n' \sim 0.6$ the uniform solution becomes suddenly more favorable (see also Fig. 7). Notice that this density is well inside the MC coexistence region ($0 < n' < 1$) showing the uniform solution stabilization effect.

It is important to remark that the whole behavior can change if the surface energy σ had a strong density dependence. For this reason the interpretation of B phase as a metal should be taken with caution since in general in a metal the surface energy will depend strongly on density. Specific examples will be treated in paper II.

-
- ¹ in *Phase separation in cuprate superconductors*, edited by K. A. Muller and G. Benedek (World Scientific, Singapore, 1992).
- ² in *Phase separation in cuprate superconductors*, edited by E. Sigmund and K. A. Muller (Springer-Verlag, Berlin, 1993).
- ³ A. Moreo, S. Yunoki, and E. Dagotto, *Science* **283**, 2034 (1999).
- ⁴ Of course quantum effects can not be neglected at the microscopic level of the PS phenomena but can be neglected at the mesoscopic level of the large clusters of particles forming the inhomogeneities.
- ⁵ E. Nagaev, *Physics of magnetic semiconductors* (MIR, Moscow, 1983).
- ⁶ E. Nagaev, A. I. Podel'shchikov, and V. E. Zil'bewareg, *J. Phys.: Condens. Matter* **10**, 9823 (1998).
- ⁷ U. Löw, V. J. Emery, K. Fabricius, and S. A. Kivelson, *Phys. Rev. Lett.* **72**, 1918 (1994).
- ⁸ C. Castellani, C. Di Castro, and M. Grilli, *Phys. Rev. Lett.* **75**, 4650 (1995).
- ⁹ M. Y. Kagan, K. I. Kugel, and D. I. Khomskii, *cond-mat/0001245* (unpublished).
- ¹⁰ E. Wigner, *Phys. Rev.* **46**, 1002 (1934).
- ¹¹ G. D. Mahan, *Many Particle Physics* (Plenum, New York, 1990).
- ¹² The usual definition of compressibility is given by $\kappa = -V^{-1}dV/dp$. This is related to our compressibilities by $k = n^2\kappa$.
- ¹³ M. Uehara, S. Mori, C. Chen, and S.-W. Cheong, *Nature* (London) **399**, 560 (1999).
- ¹⁴ D. E. Cox *et al.*, *Phys. Rev. B* **57**, 3305 (1998).
- ¹⁵ W. Jones and N. March, *Theoretical solid state physics, Vol. II*, (Wiley Interscience, New York, 1973).